Chaos, Solitons and Fractals 178 (2024) 114310

Contents lists available at ScienceDirect

Chaos, Solitons and Fractals

journal homepage: www.elsevier.com/locate/chaos

Analysis of vibrational resonance in an oscillator with exponential mass variation

T.O. Roy-Layinde [a], K.A. Omoteso [b], U.H. Diala [b,*], J.A. Runsewe [a], J.A. Laoye [a]

[a] Department of Physics, Olabisi Onabanjo University, Ago-Iwoye, Ogun State, Nigeria
[b] Department of Electrical and Electronic Engineering, University of Derby, Markeaton Street, Derby, United Kingdom

ARTICLE INFO

Keywords:
Algorithm
Mass distribution
Nonlinear system
Perturbation
Resonance

ABSTRACT

This study investigated vibrational resonance (VR) in a Duffing-type oscillator with position-dependent mass (PDM) distribution defined by spatially varying exponential function. The role of two PDM parameters, the fixed rest mass m_0 and nonlinear strength k on observed resonances was investigated from the analytical and numerical computation of response amplitude Q, which is a measure of the amplification of a low-frequency (LF) signal through the introduction and modulation of a high-frequency (HF) signal in a weakly driven nonlinear system. The method of direct separation of motion was used to analytically compute the response amplitude, while the numerically computed response amplitude was obtained from the Fourier spectrum of the output signal. Single resonance peaks with good agreement between the numerically and the analytically computed responses were observed for the traditional HF-induced VR and the PDM-induced resonances. The results demonstrated that spatial mass perturbation can play the roles of HF signals typically used in traditional VR setups. The results of this investigation corroborate earlier reports that stated PDM parameters can complement the HF signal to control the observed resonance peaks. However, the exponentially varying PDM parameters did not initiate double or multiple resonances as reported for other mass distributions such as the regular mass function and the doubly-singular mass function. This study communicates that the nature of the PDM distribution actually determines the possibility of generating new peaks from observed resonances.

1. Introduction

Nonlinear dynamics include methods of analyzing the behavior of physical systems that are often presented as differential equations [1]. The extensive application of nonlinear science to a variety of fields has attracted attention of researchers in many fields of science. These include areas like biology, medicine and social sciences. Low-order systems modeled as nonlinear ordinary differential equations are known to exhibit a variety of intriguing behaviors resulting in the emergence of strange attractors and other phenomena, one of which is resonance [2]. Nonlinearity is essential in most systems, particularly in experimental conditions. In real systems, nonlinearity can manifest in a variety of ways, including physical, structural, frictional or geometrical [3]. A source of nonlinearity often overlooked is the reactive force, particularly in systems with a variable mass due to its tendency to introduce complexity into simple physical problem with constant mass.

The dynamics of variable-mass systems require a modification to the well-known Newtonian dynamics of constant-mass systems by accounting for an additional non-conservative generalized force called the reactive force. This results from the effect of the addition/seperation of a number of particles of a system or a significant mass change over time. The contribution of the reactive force depends on the nature of the mass variation. The mass variation could be in form of position, time or velocity. The reactive force is described theoretically as the product of functions of mass variation and relative velocity of mass added or separated from the system. Several forms of mass variation functions have been studied in systems with variable mass whose associated reactive force is a nonlinear function of relative velocity of mass variation [4,5], particularly in semiconductor theory [6,7], polarons [8] and quantum dots [9,10].

In many real systems encountered in nature and technology, the variation in mass results from accretion (or ablation) processes which manifest as addition (or removal) of particles to (or from) a mass as the particle changes in position, time or velocity [11]. For instance, during the formation of an iceberg, when snow falls on the surface of a floating iceberg, it freezes and the mass of the iceberg increases. However, the heat from the Sun's rays melt the surface ice thereby decreasing the mass of the iceberg [12]. In the transportation mechanisms used in manufacturing industries such as rotors and conveyor belts, loading and

* Corresponding author.
E-mail address: U.Diala@derby.ac.uk (U.H. Diala).

https://doi.org/10.1016/j.chaos.2023.114310
Received 16 August 2023; Received in revised form 24 October 2023; Accepted 23 November 2023
Available online 2 December 2023

unloading processes continually alter the mass of products on the conveyor belt. Also, the mass of a falling meteorite decreases as it passes the Earth's burning atmosphere, whereas the Earth's mass increases when the meteorite drops on its surface [12]. Rockets continually burn fuel to gain thrust which leads to mass decrease over time [13]. The nonlinearity introduced into the dynamics of a variable mass system has the potential to affect the system's dynamics. For instance, the order of nonlinearity influences the amplitude and phase change in a lightly damped oscillator with a variable mass [14]. Mass variation initiates other complex dynamics such as bifurcation, chaos, hysteresis, multistability and resonance [15].

Resonance is a fundamental phenomenon demonstrated by linear and nonlinear dynamical systems. Traditionally, a system is considered to be at resonance if its response amplitude becomes amplified upon introducing small perturbation with a frequency close to the system's natural frequency [16]. The phenomena of resonance, particularly in nonlinear systems, has been extended to include all forms of amplification initiated through the modulation of any of the system parameters. This definition implies frequency-matching is not a precondition for nonlinear resonance. Nonlinear resonances is applicable to multiple fields of study including neuroscience, engineering, optics, ionospheric physics, atomic physics, acoustics and laser physics. Nonlinear resonance can be initiated by different types of external forces, leading to various forms such as stochastic resonance [17], chaotic and ghost resonance [18,19] and vibrational resonance [20]. Vibrational resonance (VR) displays many analogies to the well-known phenomenon of stochastic resonance, but with a periodic external force filling the role usually played by noise [21]. Vibrational resonance occurs when a system is subjected to a bi-harmonic excitation consisting of a small-amplitude LF signal and a large-amplitude HF signal.

Following the pioneering work on VR by Landa and McClintock [20], the last two decades have seen a great amount of research output on theoretical and experimental studies on VR in monostable [20,22], bistable [23] and multistable potentials [24,25]. VR has been examined in systems modeled as excitable systems [26], coupled oscillators [27], fractional-order systems [28], electrical systems [29,30] and biological systems [31–33]. Some fascinating characteristics and possible applications of VR have been highlighted. A novel ghost vibrational resonance phenomenon was observed in a system driven by multi-frequency signals [34]. The application of VR in signal processing is well-established, and has been suggested for signal transmission, filtering and amplification [35]. VR has been suggested as a propitious technique for non-invasive, nascent bearing-fault diagnosis [36–39]. Other physical applications include information processing [40], nonlinear signal processing [40], noisy image perception [41], detection of weak-faults in rotating machines [42] and synthetic gene networks [43]. These studies have enormous contributions to our knowledge of the VR phenomenon, its underlying mechanism, and possible applications.

However, most of these studies assumed the systems possessed a constant mass, and little attempt have been made to investigate VR in systems with a variable mass. In a noteworthy study, Roy-Layinde et al. [44] examined VR in a simple, but general, position-dependent mass system with a regular mass function consisting of a constant mass (mass amplitude) and a quadratic spatial nonlinearity. A general theoretical framework for dealing with VR in PDM systems was developed and the variable mass parameters were shown to play essential complementary roles to the high-frequency signal. The approach yielded similar results in the analysis of VR in a PDM oscillator with doubly singular mass distribution describing the vibrational inversion mode of NH_3 molecule [45]. However, the mass functions considered in both literature only admit certain position values with unavoidable singularities, limiting the number of applicable physical systems. Hence, a mass distribution with large admissibility is suggested. We note that different mass distributions abound and their effect on observed system dynamics may vary [46]. Motivated by the remarkable results of the aforementioned studies, we extend the gains by redefining the mass distribution as an exponential distribution. The exponential function describes the mass as a regular mass-function on a whole real line with large number of applications. In this paper, we investigate vibrational resonance in a Duffing-type PDM system with an exponential mass function.

2. The model

We consider an archetypical periodically driven nonlinear system which describes the dynamics of a position-dependent point mass, defined by exponential mass distribution. The carefully interpreted generalized Newton's second law of motion for the classical PDM systems from analytical mechanics is known to contain an extra non-conservative generalized force due to the mass variation termed the reactive force, $R_{PDM}(x,\dot{x};t)$. The reactive force is a quadratic function of velocity and is linearly proportional to the mass gradient; $R_{PDM}(x,\dot{x},t) = \frac{1}{2}\frac{dm(x)}{dx}$ [4,5].

The Euler–Lagrange equation which encodes the dynamics of the variable mass $m(x)$ is given by

$$\frac{d}{dt}\left(\frac{\partial L}{\partial \dot{x}}\right) - \frac{\partial L}{\partial x} = \phi, \tag{1}$$

where

$$L(x,\dot{x};t) = T - V(x) = \frac{1}{2}m(x)\dot{x}^2 - V(x) \tag{2}$$

is the Lagrangian $L(x,\dot{x};t)$ associated to the Newton's equation of motion of the form

$$\begin{aligned} F(x,\dot{x};t) &= F(x;t) + R_{PDM}(x,\dot{x};t) \\ &= -\frac{dV(x)}{dx} + \phi \end{aligned} \tag{3}$$

[46–48]. In Eqs. (1), (2) and (3), the overdot indicates differentiation with respect to time. $T = \frac{1}{2}m(x)\dot{x}^2$ is the kinetic energy of the system, $V(x)$ is the system potential, and $\phi(= -\alpha\dot{x} + F_{ext})$ is the net dissipative force consisting of the damping term $\alpha\dot{x}$ and the external driving force F_{ext}. The Newton's equation of motion (Eq. (3)) form of the Euler–Lagrange equation (Eq. (1)) for a PDM system with inertial force $F(x;t) = m(x)\ddot{x}$ can easily be shown to be

$$m(x)\ddot{x} + \frac{1}{2}m'(x)\dot{x}^2 + \frac{dV(x)}{dx} = \phi. \tag{4}$$

By substituting for ϕ in Eq. (4) and dividing through by $m(x)$, we have

$$\ddot{x} + \frac{1}{2}\frac{m'(x)}{m(x)}\dot{x}^2 + \frac{\alpha}{m(x)}\dot{x} + \frac{1}{m(x)}\frac{dV(x)}{dx} = \frac{F_{ext}}{m(x)}. \tag{5}$$

Eq. (5) is the model of a dissipative particle with position-dependent variable mass evolving in a potential of the form

$$V(x) = \frac{1}{2}m(x)\omega_0^2x^2 + \frac{1}{4}\beta x^4. \tag{6}$$

We consider a variable mass with position-dependent mass distribution of the form

$$m(x) = m_0e^{\frac{kx}{2}} \tag{7}$$

where m_0 is the particle rest mass (mass at $k = 0$), and k is a constant factor resulting from the particle accretion or ablation process [46]. The constants m_0 and $\frac{1}{k}$ are expressed in mass and position units, respectively. The mass distribution (Eq. (7)) is referred to as an exponential mass function. By substituting Eqs. (6) and (7) in Eq. (5), the system with a variable mass can be modeled as a driven nonlinear dissipative system of the form

$$\ddot{x} + b(x)\dot{x}^2 + c(x)\dot{x} + d(x) = h(x), \tag{8}$$

where

$$\begin{aligned} b(x) &= \frac{1}{2}\frac{m'(x)}{m(x)} = \frac{1}{4}\frac{km_0e^{\frac{kx}{2}}}{m(x)} = \frac{k}{4}, \\ c(x) &= \frac{\alpha}{m(x)} = \frac{\alpha e^{\frac{-kx}{2}}}{m_0}, \end{aligned} \tag{9}$$

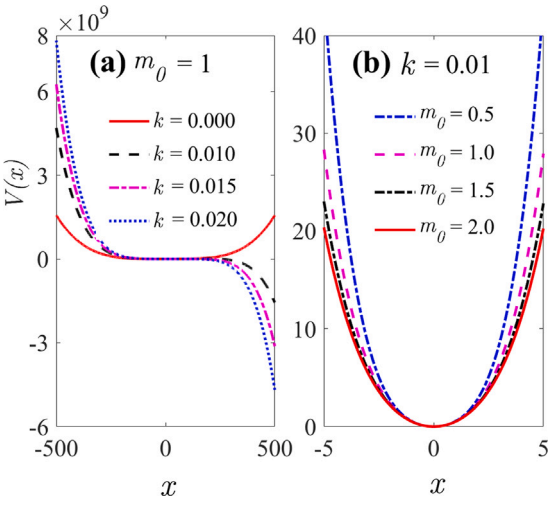

Fig. 1. The PDM system potential structure computed from Eq. (13) for different parameter values of the variable mass (a) when the fixed rest mass $m_0 = 1$ and $k = [0.0\ 0.01\ 0.015\ 0.02]$ (b) when the nonlinear mass strength $k = 0.01$ and $m_0 = [0.5\ 1.0\ 1.5\ 2.0]$. Other parameters are set as $\omega_0 = 1, \beta = 0.1$.

$$d(x) = \frac{1}{m(x)}\frac{dV(x)}{dx} = \omega_0^2 x + \frac{k}{4}\omega_0^2 x^2 + \frac{\beta e^{\frac{-kx}{2}}}{m_0}x^3,$$
$$h(x) = F_{ext}\frac{e^{\frac{-kx}{2}}}{m_0}.$$

If we define the external drive as an additive bi-harmonic signal of the form $F_{ext} = f\cos\omega t + g\cos\Omega t$, comprising of a slow periodic input signal with frequency ω and a fast driving signal with high-frequency Ω, where ($\Omega \gg \omega$), then Eq. (8) describing the PDM system with an exponential mass function can be written as

$$\ddot{x} + \frac{k}{4}\dot{x} + \frac{\alpha}{m_0}e^{\frac{-kx}{2}}\dot{x} + \omega_0^2 x + \frac{k}{4}\omega_0^2 x^2 + \frac{\beta}{m_0}e^{\frac{-kx}{2}}x^3 = (f\cos\omega t + g\cos\Omega t)\frac{e^{\frac{-kx}{2}}}{m_0}. \tag{10}$$

Eq. (10) can be considered as a model of bi-harmonically forced steel beam, plasma ionization and nonlinear electronic circuits with variable mass.

By choosing the first two terms of the power series of $e^{\frac{-kx}{2}}$, such that $e^{\frac{-kx}{2}} \approx \left(1 - \frac{kx}{2}\right)$, we obtain an approximate form of Eq. (7), which is valid for small value of k and more amenable to the perturbation technique of Direct Separation of Motion, given by

$$\ddot{x} + \frac{k}{4}\dot{x}^2 + \frac{\alpha}{m_0}\left(1 - \frac{kx}{2}\right)\dot{x} + {\omega_0}^2 x + \frac{k}{4}{\omega_0}^2 x^2 + \frac{\beta}{m_0}\left(1 - \frac{kx}{2}\right)x^3 = (f\cos\omega t + g\cos\Omega t)\frac{1}{m_0}\left(1 - \frac{kx}{2}\right). \tag{11}$$

Eq. (11) can be expanded as

$$\ddot{x} + \frac{k}{4}\dot{x}^2 + \frac{\alpha}{m_0}\dot{x} - \frac{\alpha k}{2m_0}x\dot{x} + \omega_0^2 x + \frac{k}{4}\omega_0^2 x^2 + \frac{\beta}{m_0}x^3 - \frac{\beta k}{2m_0}x^4 = (f\cos\omega t + g\cos\Omega t)\frac{1}{m_0}\left(1 - \frac{kx}{2}\right) \tag{12}$$

Hence, the PDM system (Eq. (10)) can be approximated as Eq. (12). The system's potential $V(x)$ in the presence of an exponentially varying PDM is thus

$$V(x) = \frac{\omega_0^2}{2}x^2 + \frac{k}{12}\omega_0^2 x^3 + \frac{\beta}{4m_0}x^4 - \frac{\beta k}{10m_0}x^5. \tag{13}$$

We note that when the mass is constant ($k = 0$), the system is reduced to the well-known Duffing oscillator whose fascinating dynamics exhibits chaotic behavior, hysteresis, and resonance.

The potential of the approximated PDM system with exponentially varying mass (Eq. (12)) given by Eq. (13), is shown in Fig. 1. The PDM system has an asymmetric single-well for all positive values of ω_0^2. The shape of the potential remains unchanged for four values of PDM parameters $k = [0\ 0.01\ 0.015\ 0.02]$ and $m_0 = [0.5\ 1.0\ 1.5\ 2.0]$, as shown in Fig. 1(a) and Fig. 1(b), respectively. More importantly, the effect of the parameter, k on the shape of the system's potential is clear from Fig. 1(a), especially, when increased from $k = 0.010$ to $k = 0.020$. Therefore, examining the impact of large values of k is immaterial. The effect of the HF signal on the system potential structure can be observed from the potential of the slow oscillation, which is considered the effective potential of the PDM.

3. Methods

Techniques that provide reliable proof for the existence of vibrational resonance in PDM systems were used, particularly independent analytical and numerical methods. The vibrational resonance phenomenon is examined through a characteristic term called response factor Q, which provides an insight into how the cooperation between the parameters of the external driving signals of a nonlinear system results in amplified output. Usually, a bell-shaped response curve is indicative of resonance. Traditionally, vibrational resonance (VR) is achieved by the variation of the response amplitude with respect to the parameters of the HF signal (g, Ω).

3.1. Analytical method

Here, we apply the standard perturbation method of Direct Separation of Motion (DSM) which is well described in [49,50], to retrieve the dynamics of the system with respect to the influence of the external high-frequency (HF) signal by splitting system's equation of motion (12) into slow and fast motions. To apply the DSM method, we assume the system's response comprises of a slow component $y(t)$ and a fast component $z(t,\tau)$, where τ is the fast time ($\tau = \Omega t$) of the HF drive with frequency Ω ($\Omega \gg \omega$). We set out to obtain a pair of integro-differential equations, which describes the equations of slow oscillations as well as the fast vibrations and the superposition of their solutions completely solves the PDM system presented in Eq. (12). Therefore we assume

$$x(t) = y(t) + z(t,\tau). \tag{14}$$

Substituting Eq. (14) into the PDM oscillator of Eq. (12), we can write

$$\ddot{y} + \ddot{z} + \frac{k}{4}(\dot{y}+\dot{z})^2 + \frac{\alpha}{m_0}(\dot{y}+\dot{z}) - \frac{\alpha k}{2m_0}(y+z)(\dot{y}+\dot{z}) + \omega_0^2(y+z) + \frac{k\omega_0^2}{4}(y+z)^2 + \frac{\beta}{m_0}(y+z)^3 - \frac{\beta k}{2m_0}(y+z)^4 = (f\cos\omega t + g\cos\Omega t)\frac{1}{m_0}(1 - \frac{k}{2}(y+z)). \tag{15}$$

Eq. (15) can be expanded to give

$$\ddot{y} + \ddot{z} + \frac{k}{4}\dot{y}^2 + \frac{k}{4}\dot{z}^2 + \frac{k}{2}\dot{z}\dot{y} + \frac{\alpha}{m_0}\dot{y} + \frac{\alpha}{m_0}\dot{z} - \frac{\alpha k}{2m_0}(y\dot{y} + z\dot{y}) - \frac{\alpha k}{2m_0}(y\dot{z} + z\dot{z}) + \omega_0^2 y + \omega_0^2 z + \frac{k\omega_0^2}{4}(y^2 + 2yz + z^2) + \frac{\beta}{m_0}(y^3 + 3y^2 z + 3yz^2 + z^3) - \frac{\beta k}{2m_0}(y^4 + 4y^3 z + 6y^2 z^2 + 4yz^3 + z^4) = (f\cos\omega t + g\cos\Omega t)\frac{1}{m_0}(1 - \frac{k}{2}(y+z)). \tag{16}$$

We note that the z component is rapidly oscillating with period 2π, while the slow component, $y(t)$ is assumed to be periodic with period $T = \frac{2\pi}{\omega}$. Hence, we average both sides of Eq. (16) with respect to the fast time by taking the mean values (denoted by an overline) of the fast components, which gives

$$\ddot{y} + \ddot{\bar{z}} + \frac{k}{4}\dot{y}^2 + \frac{k}{4}\overline{\dot{z}^2} + \frac{k}{2}\bar{z}\dot{y} + \frac{\alpha}{m_0}\dot{y} + \frac{\alpha}{m_0}\dot{\bar{z}}$$

$$- \frac{\alpha k}{2m_0}(y+\overline{z})\dot{y} - \frac{\alpha k}{2m_0}(y+\overline{z})\dot{\overline{z}} + \omega_0^2 y + \omega_0^2\overline{z} + \frac{kw_0^2}{4}(y^2 + 2y\overline{z} + \overline{z^2})$$
$$+ \frac{\beta}{m_0}(y^3 + 3y^2 z + 3y\overline{z^2} + \overline{z^3}) - \frac{\beta k}{2m_0}(y^4 + 4y^3\overline{z} + 6y^2\overline{z^2} + 4y\overline{z^3} + \overline{z^4})$$
$$= (f\cos\omega t + \overline{g\cos\Omega t})\frac{1}{m_0}(1 - \frac{k}{2}(y+\overline{z})). \quad (17)$$

By factorizing like terms, Eq. (17) becomes

$$\ddot{y} + \frac{k}{4}\dot{y}^2 + \frac{\alpha}{m_0}\left(1 - \frac{k\overline{z}}{2}\right)\dot{y} - \frac{\alpha k}{2m_0}y\dot{y}$$
$$+ \left(\omega_0^2 + \frac{k\omega_0^2}{2}\overline{z} + \frac{3\beta}{m_0}\overline{z^2} - \frac{2\beta k}{m_0}\overline{z^3}\right)y + \left(\frac{k\omega_0^2}{4} + \frac{3\beta}{m_0}\overline{z} - \frac{3\beta k}{m_0}\overline{z^2}\right)y^2$$
$$+ \left(\frac{\beta}{m_0} - \frac{2\beta k\overline{z}}{m_0}\right)y^3 - \left(\frac{\beta k}{2m_0}\right)y^4 + \overline{\dot{z}} + \frac{k}{4}\overline{\dot{z}^2}$$
$$+ \left(\frac{k}{2}\dot{y} + \frac{\alpha}{m_0} - \frac{\alpha k}{2m_0}(y+\overline{z})\right)\overline{\dot{z}} + +\omega_0^2\overline{z} + \frac{k\omega_0^2}{4}\overline{z^2} + \frac{\beta}{m_0}\overline{z^3} - \frac{\beta k}{2m_0}\overline{z^4}$$
$$= (f\cos\omega t + \overline{g\cos\Omega t})\frac{1}{m_0}(1 - \frac{k}{2}(y+\overline{z})) \quad (18)$$

The mean value of $z(\tau)$ w.r.t the fast time τ is given by

$$\overline{z} = \frac{1}{2\pi}\int_0^{2\pi} z d\tau = 0, \quad (19)$$

and $\overline{g\cos\Omega t} = 0$, so that Eq. (18) becomes

$$\ddot{y} + \frac{k}{4}\dot{y}^2 + \frac{\alpha}{m_0}\dot{y} - \frac{\alpha k}{2m_0}y\dot{y} + \left(\omega_0^2 + \frac{3\beta}{m_0}\overline{z^2} - \frac{2\beta k}{m_0}\overline{z^3}\right)y$$
$$+ \left(\frac{k\omega_0^2}{4} - \frac{3\beta k}{m_0}\overline{z^2}\right)y^2 + \left(\frac{\beta}{m_0}\right)y^3 + \left(\frac{-\beta k}{2m_0}\right)y^4$$
$$+ \frac{k\omega_0^2}{4}\overline{z^2} + \frac{\beta}{m_0}\overline{z^3} - \frac{\beta k}{2m_0}\overline{z^4} = \frac{f}{m_0}\left(1 - \frac{k}{2}y\right)\cos\omega t \quad (20)$$

Eq. (20) is the equation of the slow motion of the system which we are mostly interested in and it is one of the integro-differential equations we set out to obtain using the DSM. We would use an approximation method to obtain the mean values in the equation. This is done by first obtaining the second integro-differential equation, which is the equation of the fast oscillation z, by subtracting the equation of slow component y (Eq. (20)) from the equation of the composite system x (Eq. (12)). Hence, the system's equation for the fast oscillation is

$$\ddot{z} + \frac{k}{4}\dot{z}^2 + \left(\frac{k}{2}\dot{y} + \frac{\alpha}{m_0} - \frac{\alpha k}{2m_0}(y + (z-\overline{z}))\right)\dot{z}$$
$$+ \left(\omega_0^2 - \frac{\alpha k\dot{y}}{2m_0} + \frac{k\omega_0^2 y}{2} + \frac{3\beta y^2}{m_0} - \frac{2\beta k y^3}{m_0}\right)(z-\overline{z})$$
$$+ \left(\frac{3\beta y}{m_0} - \frac{3\beta k y^2}{m_0} + \frac{k\omega_0^2}{4}\right)(z^2 - \overline{z^2})$$
$$- \left(\frac{2\beta k y}{m_0} - \frac{\beta}{m_0}\right)(z^3 - \overline{z^3}) - \frac{\beta k}{2m_0}(z^4 - \overline{z^4})$$
$$= \frac{g}{m_0}\left(1 - \frac{k}{2}(y + (z-\overline{z}))\right)\cos\Omega t - \frac{f}{m_0}\left(\frac{k}{2}(z-\overline{z})\right)\cos\omega t \quad (21)$$

Next, we obtain the mean values in Eq. (20) by applying the inertial approximation $\ddot{z} \gg \dot{z} \gg z \gg z^2$ [51], and assuming the fast component z is much faster than the slow component y so that the contribution of the slow component to the fast motion (Eq. (21) becomes negligible, that is, y and $\dot{y}$ are considered frozen in Eq. (21). Hence Eq. (21) is reduced to

$$\ddot{z} = \frac{g}{m_0}\cos\Omega t, \quad (22)$$

which has a solution

$$z = \frac{-g}{m_0\Omega^2}\cos\Omega t. \quad (23)$$

Using Eq. (23), the mean values are obtained as

$$\overline{z} = \overline{z^3} = \overline{z^5} = 0,$$

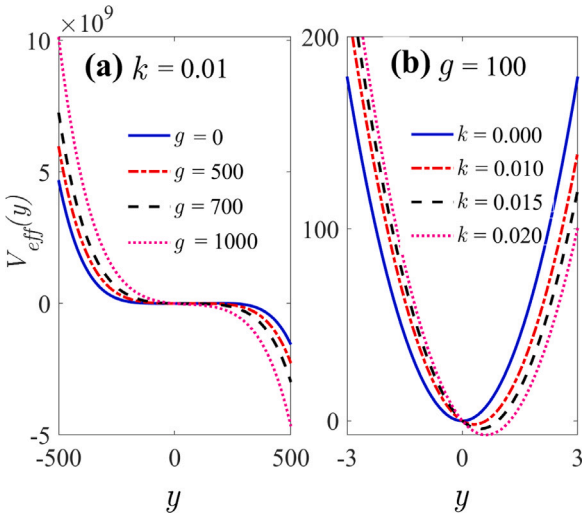

Fig. 2. The effective potential of the system computed from Eq. (27) showing the contribution of fast signal (a) when nonlinear mass strength $k = 0.01$ for four values of the HF amplitude $g = (0, 500, 700, \text{and} 1000)$ (b) when the HF amplitude $g = 100$ for four values of the mass nonlinear strength $(0.0, 0.01, 0.015, \text{and} 0.02)$. Other parameters are set as $\omega_0 = 1, \beta = 0.1, \Omega = 4\omega, \omega = 0.1$.

$$\overline{z^2} = \frac{g^2}{2m_0^2\Omega^4}, \quad \overline{z^4} = \frac{3g^4}{8m_0^4\Omega^8}, \quad \overline{\dot{z}^2} = \frac{g^2}{2m_0^2\Omega^2}. \quad (24)$$

Substituting Eq. (24) in the equation of slow motion (Eq. (20)), gives

$$\ddot{y} + \frac{k}{4}\dot{y}^2 + \frac{\alpha}{m_0}\dot{y} - \frac{\alpha k}{2m_0}y\dot{y} + C_1 y + C_2 y^2 + C_3 y^3$$
$$+ C_4 y^4 + C_0 = \frac{f}{m_0}\left(1 - \frac{k}{2}y\right)\cos\omega t, \quad (25)$$

where

$$C_1 = \left(\omega_0^2 + \frac{3\beta}{m_0}\overline{z^2} - \frac{2\beta k}{m_0}\overline{z^3}\right) = \omega_0^2 + \frac{3\beta g^2}{2m_0^3\Omega^4},$$
$$C_2 = \left(\frac{k\omega_0^2}{4} - \frac{6\beta k}{2m_0}\overline{z^2}\right) = \frac{k}{4}\left(\omega_0^2 - \frac{6\beta g^2}{m_0^3\Omega^4}\right),$$
$$C_3 = \left(\frac{\beta}{m_0}\right), \quad C_4 = \left(\frac{-\beta k}{2m_0}\right), \quad (26)$$
$$C_0 = \left(\frac{k\omega_0^2}{4}\overline{z^2} + \frac{\beta}{m_0}\overline{z^3} - \frac{\beta k}{2m_0}\overline{z^4}\right) = \frac{kg^2}{8m_0^2\Omega^4}\left(\omega_0^2 - \frac{3\beta g^2}{2m_0^3\Omega^4}\right)$$

The effective potential of the PDM oscillator is given as

$$V_{eff}(y) = C_0 y + \frac{1}{2}C_1 y^2 + \frac{C_2}{3}y^3 + \frac{C_3}{4}y^4 + \frac{C_4}{5}y^5. \quad (27)$$

The slow oscillation takes place about the equilibrium point y^*, which is one of the four roots of the quartic equation

$$C_4 y^{*4} + C_3 y^{*3} + C_2 y^{*2} + C_1 y^* + C_0 = 0. \quad (28)$$

If Eq. (28) has three real roots which are designated y_R^*, y_M^* and y_L^*, then for the double-well effective potential, y_R^* and y_L^* denote the right-well and left-well local minima, respectively, while y_M^* represents the middle-hump local maximum.

The effect of the HF amplitude g on the effective potential is shown in Fig. 2(a) for four values of $g = [0, 500, 700, 1000]$. The effective potential remains single-well when the system is bi-harmonically driven, and this is consistent for all chosen values of the mass nonlinear strength as shown in Fig. 2(b) for $k = [0, 0.01, 0.015, 0.02]$.

Next, we describe the system's oscillation by the motion around the equilibrium points by defining a deviation variable $Y = y - y^*$ which

is the deviation of the slow motion y from the equilibrium points y^*. Using $y = Y + y^*$ in Eq. (25) yields

$$\begin{aligned}\ddot{Y} &+ \frac{k}{4}\dot{Y}^2 + \gamma\dot{Y} - \frac{\alpha k}{2m_0}Y\dot{Y} + \omega_r^2 Y + \eta_1 Y^2 + \eta_2 Y^3 \\ &+ C_4 Y^4 + \eta_3 = \frac{f}{m_0}\left(1 - \frac{k}{2}(Y + y^*)\right)\cos\omega t,\end{aligned} \tag{29}$$

where

$$\begin{aligned}\gamma &= \frac{\alpha}{m_0}(1 - \frac{ky^*}{2}),\\ \omega_r^2 &= C_1 + 2C_2 y^* + 3C_3 y^{*2} + 4C_4 y^{*3},\\ \eta_1 &= C_2 + 3C_3 y^* + 6C_4 y^{*2},\\ \eta_2 &= C_3 + 4C_4 y^*,\\ \eta_3 &= C_4 y^{*4} + C_3 y^{*3} + C_2 y^{*2} + C_1 y^* + C_0.\end{aligned} \tag{30}$$

Assuming that $|Y| \ll 1$ for $f \ll 1$ in the long-term limit as $t \to \infty$ and discarding higher powers in the deviation Y in Eq. (29), then the approximate linear equation of motion can be written as

$$\ddot{Y} + \gamma\dot{Y} + \omega_r^2 Y = F\cos\omega t, \tag{31}$$

where ω_r is the resonant frequency and $F = \frac{f}{m_0}$ is the approximate amplitude. The steady state solution of Eq. (31) is obtained as

$$Y(t) = A_L\cos(\omega t - \Phi), \tag{32}$$

where

$$A_L = \frac{F}{\sqrt{(\omega_r^2 - \omega^2)^2 + \gamma^2\omega^2}}, \tag{33}$$

and

$$\Phi = \tan^{-1}\left(\frac{\omega^2 - \omega_r^2}{\gamma\omega}\right). \tag{34}$$

The analytically computed response amplitude is thus given as

$$Q_{ana} = \frac{A_L}{f} = \frac{1}{m_0\sqrt{(\omega_r^2 - \omega^2)^2 + \gamma^2\omega^2}}. \tag{35}$$

3.2. Numerical method

The response amplitude which characterizes the phenomenon of VR is computed numerically from the Fourier components of the output signal. The output signal is obtained by first expressing the system given by Eq. (12) as a system of coupled autonomous first order ODEs of the form

$$\begin{aligned}\dot{x} &= y \\ \dot{y} &= -\frac{k}{4}\dot{x}^2 - \frac{\alpha e^{\frac{-kx}{2}}}{m_0}\dot{x} - \omega_0^2 x - \frac{\omega_0^2 k}{4}x^2 - \frac{\beta e^{\frac{-kx}{2}}}{m_0}x^3 \\ &+ \frac{(f\cos\omega t + g\cos\Omega t)e^{\frac{-kx}{2}}}{m_0},\end{aligned} \tag{36}$$

and integrating Eq. (36) over a time interval $T_s = nT$ using the Fourth-Order Runge–Kutta scheme with a step size of $\Delta t = 0.01$, where $T\ (= \frac{2\pi}{\omega})$ is the period of oscillation of the LF (ω) external signal, and $n\ (= 1, 2, 3, \ldots)$ is the number of complete oscillations. The initial conditions $(x(0) = 0, y(0) = 1)$ were used, and the first $n = 100$ initial iterates were discarded as transient solutions. The response amplitude Q of the system is computed at the frequency of the slow input signal as the sum of the Fourier series of the output signal within a periodic window. Thus, the numerically computed response amplitude Q_{num} and the phase shift Φ are given by

$$Q_{num} = \frac{A}{F} = \frac{\sqrt{Q_s^2 + Q_c^2}}{F}, \tag{37}$$

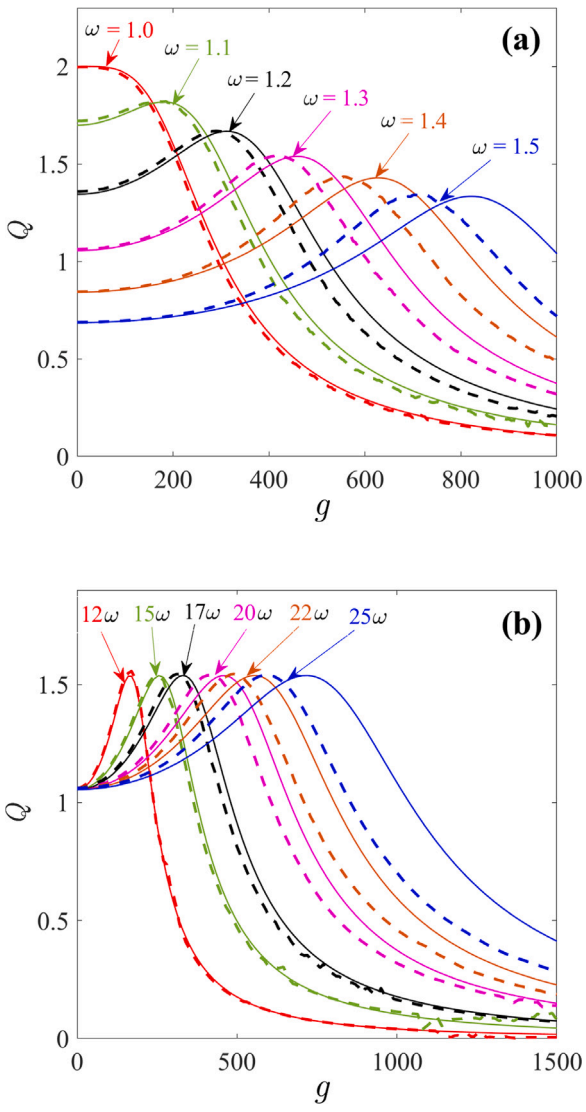

Fig. 3. Dependence of the response amplitude Q on the HF amplitude g for six values of the (a) LF term $\omega = [1.0, 1.1, 1.2, 1.3, 1.4$ and $1.5]$ when $\Omega = 20\omega$, (b) HF term $\Omega = [12\omega, 15\omega, 17\omega, 20\omega, 22\omega$ and $25\omega]$ when $\omega_0 = 1$. Other system parameters are: $\beta = 1$, $\alpha = 0.5$, $f = 0.1$, $k = 0.01$, $m_0 = 1.0$. Thick broken line represents the response curve obtained from the analytically computed response amplitude using Eq. (35) while thin continuous line of the same color represents the corresponding response curve from the numerically computed response amplitude using Eq. (37).

and

$$\Phi = \tan^{-1}\left(\frac{Q_s}{Q_c}\right), \tag{38}$$

respectively. Q_s and Q_c are respectively the Fourier sine and cosine components of the output signal x obtained as the solution of Eq. (36), and are given as

$$\begin{aligned}Q_s &= \frac{2}{nT}\int_0^{nT} x(t)\sin\omega t\ dt \\ Q_c &= \frac{2}{nT}\int_0^{nT} x(t)\cos\omega t\ dt.\end{aligned} \tag{39}$$

The numerically calculated response amplitude Q_{num}, given by Eq. (37) is then compared with the analytically computed response amplitude Q_{ana} given by Eq. (35) by superposing response curves that demonstrate how the HF signal characteristics (g, Ω) affect the system's response Q in the presence of the PDM parameters (m_0, k). Throughout our analysis, some system parameters are fixed as follows: $\beta = 1$,

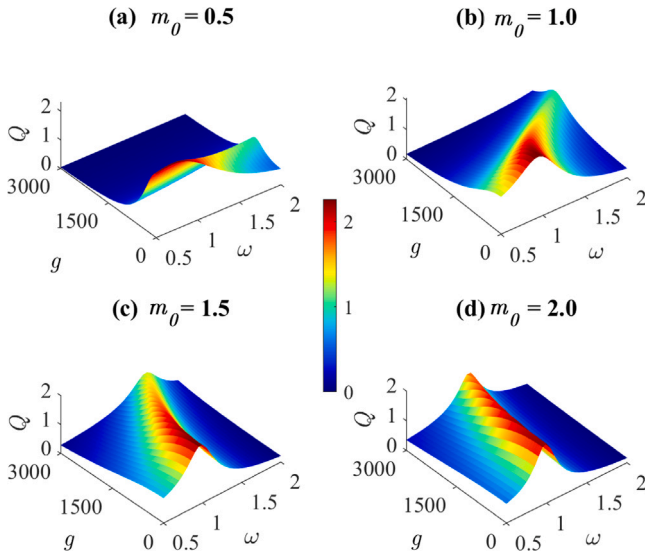

Fig. 4. 3-Dimensional variation of response amplitude on HF amplitude g and LH ω for four values of fixed rest mass (a) $m_0 = 0.5$, (b) $m_0 = 1.0$, (c) $m_0 = 1.5$ and (d) $m_0 = 2.0$. Other system parameters are: $\beta = 1$, $\alpha = 0.5$, $\omega_0 = 1$, $\Omega = 20\omega$, $f = 0.1$, $k = 0.01$.

$\alpha = 0.5$, $\omega_0 = 1$, $\omega = 1.3$, $f = 0.1$, $k = 0.01$, while the HF parameters (g, Ω) and the PDM (m_0, k) were chosen within regimes that optimizes the occurrence of the resonance phenomenon.

4. Discussion

First, we present the results obtained for the traditional VR. We showed that the PDM system with exponential mass (Eq. (12)) undergoes VR through the dependence of the response amplitude Q on the HF amplitude g as shown in Fig. 3(a) for six values of the LF parameter $\omega = [1.0, 1.1, 1.2, 1.3, 1.4, 1.5]$, when $\Omega = 20\omega$. Single resonance response curves are obtained for all values of the LF parameter.

The contribution of the LF parameter ω to the observed single resonance, is shown in Fig. 3(a) through the position of the peaks of the response curves. Fig. 3(a) shows that as LF increases, the value of the maximum response amplitude (Q_{max}) decreases, but the HF amplitude at maximum response (g_{vr}) increases. Also, the observed single-peak resonance is consistent at every value of the LF parameter for some carefully chosen values of the HF parameter Ω, for $\Omega = [12\omega, 15\omega, 17\omega, 20\omega, 22\omega, 25\omega]$ at $\omega = 1.3$ as shown in Fig. 3(b). Increasing Ω produced no obvious change in the maximum response amplitude Q_{max}, however it increases the HF amplitude at which maximum response occurs. In Figs. 3(a) and 3(b), the response curves produced from the numerically-calculated response amplitude given by Eq. (37), are presented in thick broken lines while their corresponding analytically-computed responses from Eq. (35) are presented with thin continuous lines of the same color. Clearly, the approximate analytical response amplitudes and the numerically-computed response amplitudes correspond well.

Fig. 4 presents a 3-Dimensional plot of the relationship between the response amplitude Q, HF amplitude g and LF ω as captured in Figs. 3(a) and 3(b) for four values of fixed rest mass $m_0 = [0.5, 1.0, 1.5, 2.0]$. Here, we explore the effect of the fixed rest mass on the observed resonances presented in Figs. 3(a) and 3(b). The value of the LF parameter ω at which resonance occurs is increased by increasing the fixed mass m_0 as shown in Figs. 4(a)–(d) for $m_0 = 0.5$, $m_0 = 1.0$, $m_0 = 1.5$ and $m_0 = 2.0$, respectively. Also, it can be suggested that the value of the fixed rest mass influences the HF-induced resonance through cooperation of the HF and PDM parameters. This is confirmed from the dependence of response amplitude Q on the HF amplitude g for

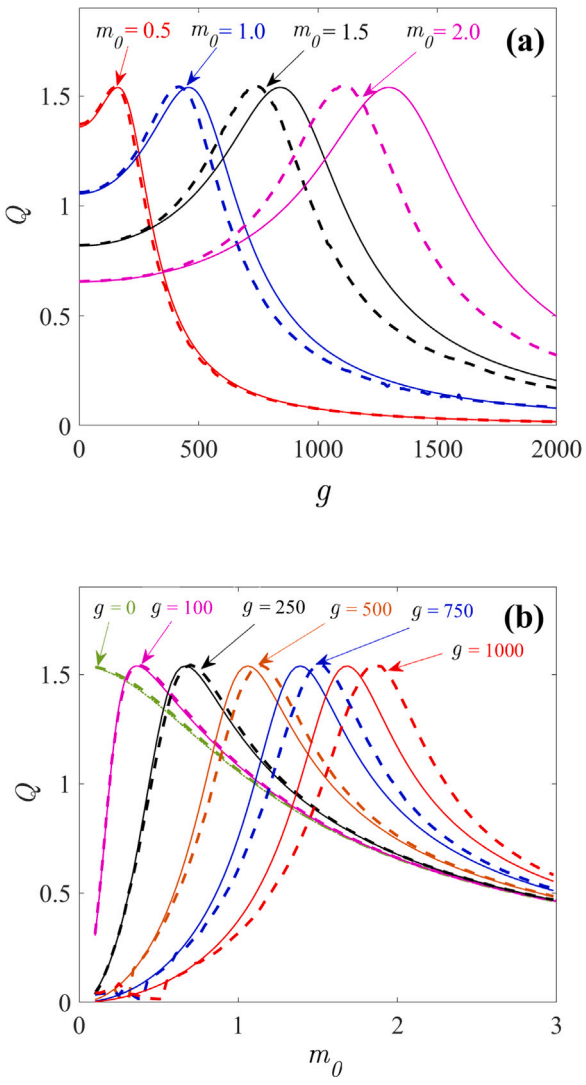

Fig. 5. Dependence of the response amplitude Q on (a) HF amplitude g for four values of fixed rest mass $m_0 = [0.5, 1.0, 1.5, 2.0]$, (b) fixed rest mass m_0 for different values of the HF amplitude $g = [0, 100, 250, 500, 750, 1000]$. Other system parameters are: $\beta = 1$, $\alpha = 0.5$, $\omega_0 = 1$, $\omega = 1.3$, $\Omega = 20\omega$, $f = 0.1$, $k = 0.01$. Thick broken line represents response curve obtained from the analytically computed response amplitude using Eq. (35) while thin continuous line of the same color represents the corresponding response curve from the numerically computed response amplitude using Eq. (37).

different fixed masses ($m_0 = 0.5, 1.0, 1.5, 2.0$) as shown in Fig. 5(a). It is observed that the fixed mass m_0 controls the value of the HF amplitude at which maximum response occurs, that is, increasing m_0 increases g_{vr}. The computed analytical and numerical results presented in Fig. 5(a) for the variation of response amplitude with HF amplitude g are in close agreement. However, the larger the fixed mass, the more the deviation between them. This deviation grows as the fixed mass increases from $m_0 = 0.5$ to $m_0 = 2.0$. This is expected due to the approximations in the analytical solution process. This validates the contributory effect of the fixed mass and is consistent with the results of Roy-Layinde et al. [44].

Next, we discuss the possibility of initiating resonance from the parameters of the exponential mass. First, we produced the response curves from the modulation of fixed mass m_0 for different values of the HF amplitude $g = [0, 100, 250, 500, 750, 1000]$ as shown in Fig. 5(b). Single resonance peaks were obtained for all values of the response amplitude. The analytically-computed response amplitude and the numerically-computed responses also show good agreement, while their deviation grows with increasing value of HF amplitude.

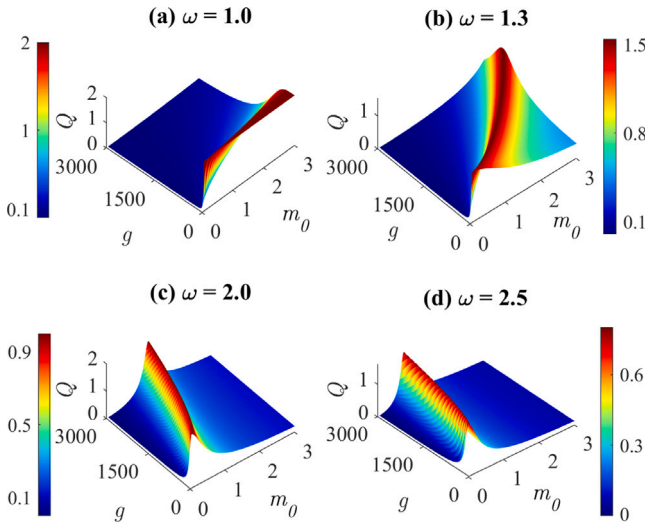

Fig. 6. 3-Dimensional variation of response amplitude on HF amplitude g and fixed rest mass m_0 for four values of LF (a) $\omega = 1.0$, (b) $\omega = 1.5$, (c) $\omega = 2.0$ and (d) $\omega = 2.5$. Other system parameters are: $\beta = 1$, $\alpha = 0.5$, $\omega_0 = 1$, $\Omega = 20\omega$, $f = 0.1$, $k = 0.01$.

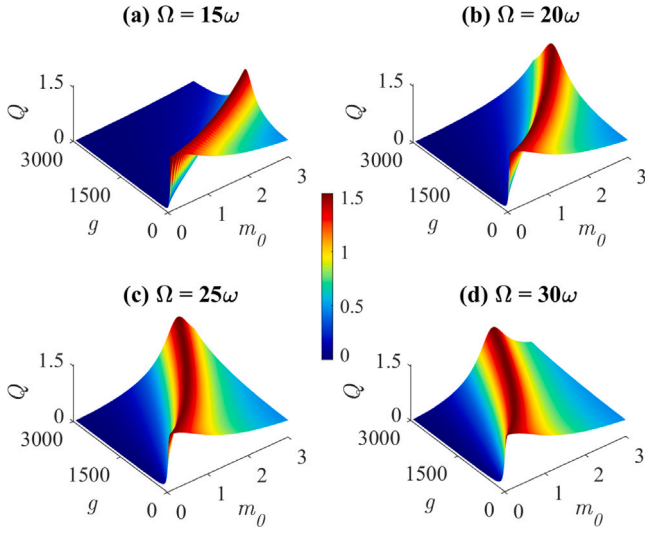

Fig. 7. 3-Dimensional variation of response amplitude Q on HF amplitude g and fixed rest mass m_0 for four values of HF (a) $\Omega = 15\omega$, (b) $\Omega = 20\omega$, (c) $\Omega = 25\omega$ and (d) $\Omega = 30\omega$. Other system parameters are: $\beta = 1$, $\alpha = 0.5$, $\omega_0 = 1$, $\omega = 1.3$, $f = 0.1$, $k = 0.01$.

From the foregoing, single resonances were obtained by modulating the HF parameter for different values of the fixed mass (see Fig. 5(a)) and by modulating the fixed mass m_0 for different values of the HF amplitude (see Fig. 5(b)). This is shown on a 3-Dimensional plot of the variation of response amplitude Q with respect to the HF amplitude and fixed mass, for four values of the LF parameter $\omega = 1.0, 1.3, 2.0, 2.5$, presented in Figs. 6(a)–(d), respectively. The single resonance peaks form a continuous ridge-shape band across the $g - m_0$ plane. The position of the resonance ridge on the plane is dependent on the LF parameter. The resonance ridge moves from one extreme of the plane to the other as ω is increased from $\omega = 1.0$ to $\omega = 2.5$, when the HF parameter is set at $\Omega = 20\omega$.

Figs. 7(a)–(d) present similar 3-Dimensional plot to Fig. 6 for four values of the HF parameter, $\Omega = 15\omega$, $\Omega = 20\omega$, $\Omega = 25\omega$ and $\Omega = 30\omega$, respectively, where $\omega = 1.3$. Again, the ridge-shaped resonance band move across the $g - m_0$ plane as the HF parameter is increased from 15Ω to 30Ω. This shows that resonance can be induced from both parameters of the plane. Furthermore, we showed in Figs. 8 and 9 that the HF parameter Ω can also induce resonance much like the HF amplitude g with 3-Dimensional plots(Q vs Ω vs m_0).

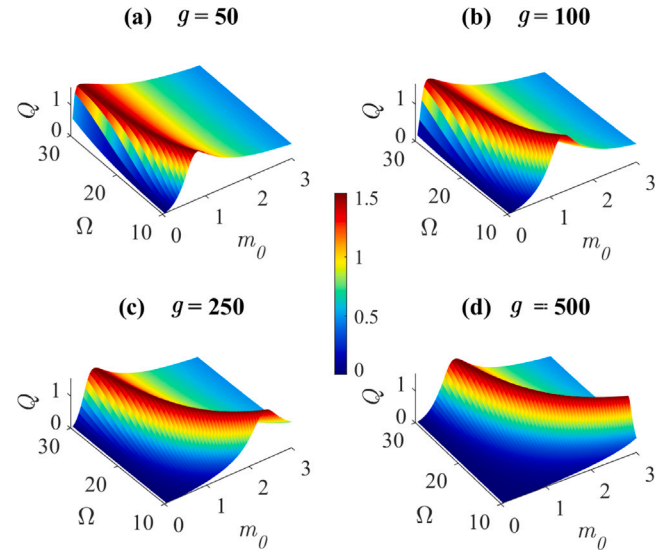

Fig. 8. 3-Dimensional variation of response amplitude Q on HF Ω and fixed rest mass m_0 for four values of HF amplitude (a) $g = 50$, (b) $g = 100$, (c) $g = 250$ and (d) $g = 500$. Other system parameters are: $\beta = 1$, $\alpha = 0.5$, $\omega_0 = 1$, $\omega = 1.3$, $f = 0.1$, $k = 0.01$.

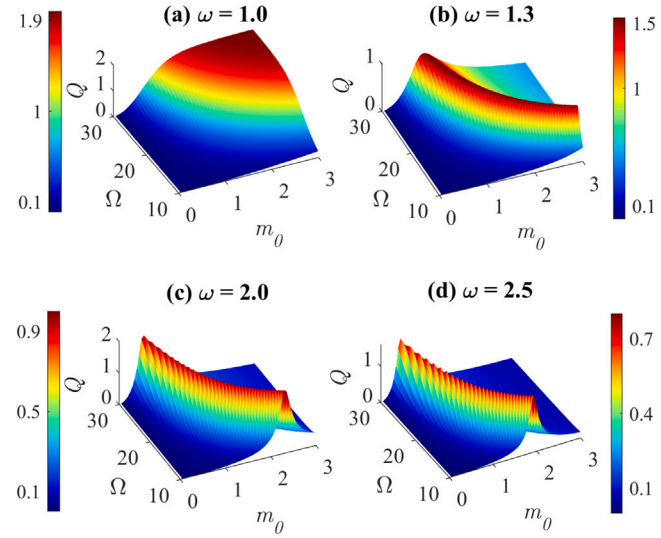

Fig. 9. 3-Dimensional variation of response amplitude Q on HF Ω and fixed rest mass m_0 for four values of HF amplitude (a) $\omega = 1$, (b) $\omega = 1.3$, (c) $\omega = 2.0$ and (d) $\omega = 2.5$. Other system parameters are: $\beta = 1$, $\alpha = 0.5$, $\omega_0 = 1$, $\omega = 1.3$, $f = 0.1$, $k = 0.01$.

Fig. 8 depicts the dependence of the response amplitude Q on HF Ω and fixed mass m_0 for four values of the HF amplitude $g = [50, 100, 250, 500]$, while Fig. 9 shows the dependence of the response amplitude Q on HF Ω and fixed mass m_0 for four values of LF $\omega = [1.0, 1.3, 2.0, 2.5]$. In these Figures, single peak resonances, controllable by the fixed mass m_0, were observed. While this is not a new result, the cooperation with the PDM parameter m_0 re-validate the role of the PDM parameter as a control parameter in VR. Finally, we examined the role of the mass nonlinear strength k in accordance with the achieved results for the fixed mass m_0. Since the system's response depends on the HF amplitude g and fixed rest mass m_0, we first present the role of the mass nonlinear strength on induced resonances, for four values of the mass nonlinear strength, $k = [0.0, 0.01, 0.02, 0.04]$ as shown in Figs. 10(a) and 10(b), respectively. When $k = 0$, the system becomes a Duffing oscillator and produces a single resonance. Figs. 10(a) and

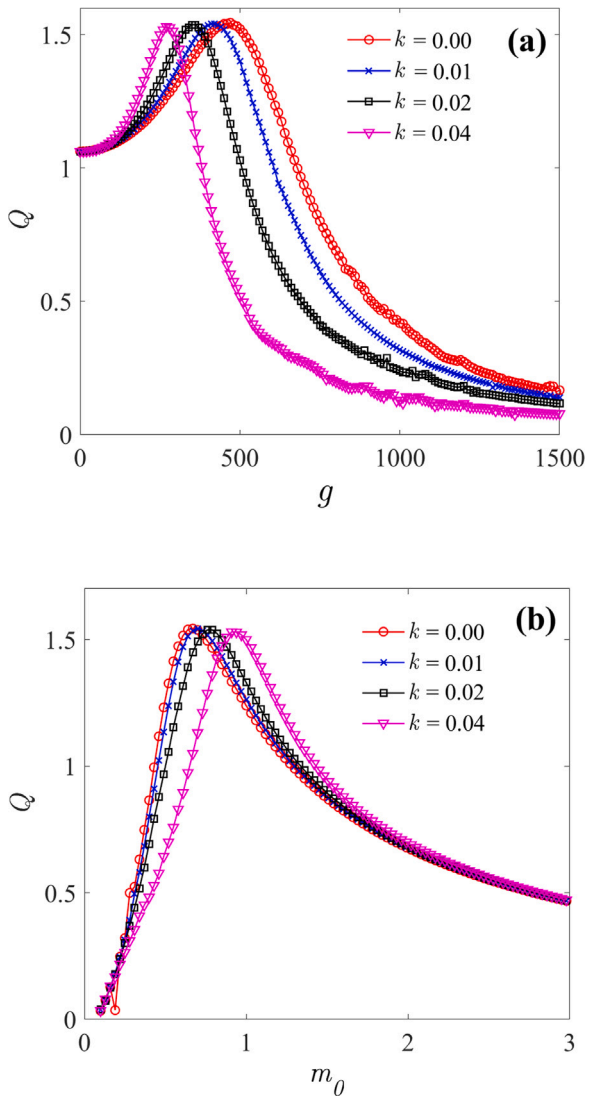

Fig. 10. (a) Dependence of the response amplitude Q, numerically computed from Eq. (37) on (a) HF amplitude g for four values of mass nonlinear strength ($k = 0, 0.01, 0.02,$ and 0.04) when $m_0 = 1$, (b) fixed rest mass m_0 for four values of mass nonlinear strength ($k = 0, 0.01, 0.02,$ and 0.04) when $g = 250$. Other system parameters are: $\beta = 1$, $\alpha = 0.5$, $\omega_0 = 1$, $\omega = 1.3$, $\Omega = 20\omega$, $f = 0.1$.

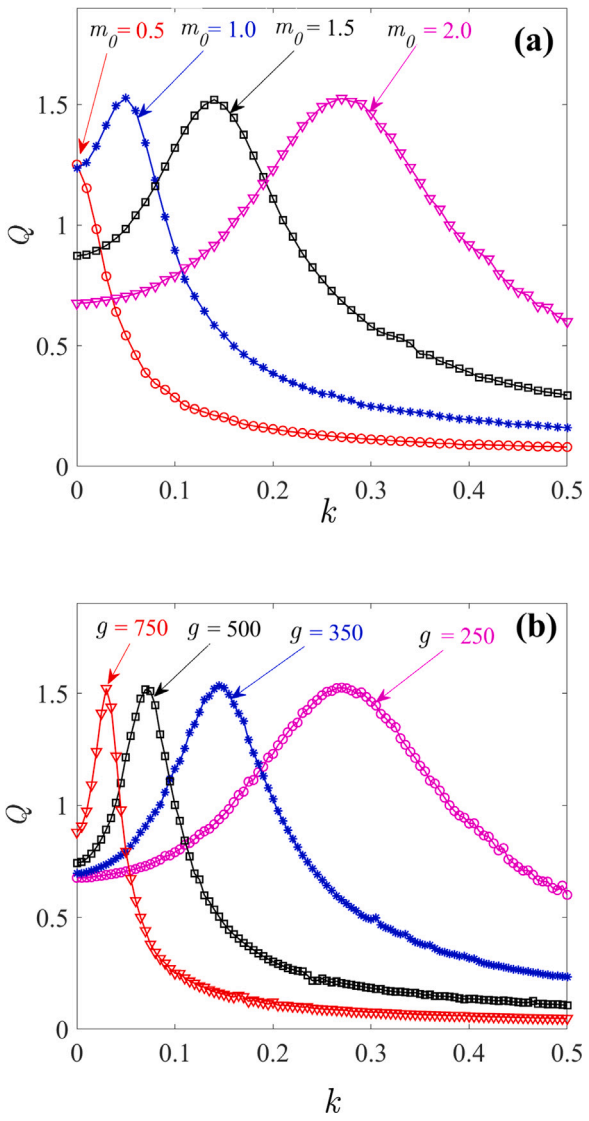

Fig. 11. Variation of response amplitude Q on mass nonlinear strength k for four values of (a) fixed rest mass $m_0 = [0.5, 1.0, 1.5, 2.0]$ at $g = 250$, (b) HF amplitude $g = [250, 350, 500, 750]$ at $m_0 = 2$. Other system parameters are: $\beta = 1$, $\alpha = 0.5$, $\omega_0 = 1$, $\omega = 1.3$, $\Omega = 20\omega$, $f = 0.1$.

10(b) show that the nature of the vibrational resonance is not affected by the system's variable mass. This is evident from the fact that just one resonance was obtained for each value of the nonlinear strength that was taken into consideration. Although, the nonlinear strength did not amplify the observed VR, the amount at which resonance occurred for the modulated system parameter, that is, g_{vr} and $m_{0_{vr}}$, are controlled by it. Hence, we remark that both PDM parameters (m_0, k) can be effectively employed to control observed resonances.

Since we have shown that the fixed mass m_0 can induce resonance in a PDM system, it is pertinent to investigate the possibility of inducing resonance by modulating the mass nonlinear strength k. This is done by modulating k to achieve resonance, as presented, for the dependence of the response amplitude on the PDM nonlinear strength k in Fig. 11(a) for four values of the fixed mass $m_0[= 0.5, 1.0, 1.5, 2.0]$ and in Fig. 11(b), for four values of the HF amplitude $g = [250, 350, 500, 750]$. Clearly, the PDM nonlinear strength also induced resonance. The k-induced single-peak resonance can also be controlled by other system parameters. The value of the PDM nonlinear strength at which maximum enhancement is achieved k_{vr}, is increased by increasing the fixed mass m_0 as shown in Fig. 11(a), and by decreasing the HF amplitude g as presented in Fig. 11(b).

In the presence of the HF signal, both PDM parameters cooperate to produce and control the resonance effect in a PDM system (shown in Fig. 11(a)). This is well highlighted by a 3-Dimensional plot of Q vs m_0 vs k presented in Fig. 12(a). The ridge-shaped continuous resonance peaks traverses across the (m_0, k)-plane, which shows both parameters can induce as well as control resonance. Similarly, a 3-Dimensional surface plot of Q vs g vs k, complementing the result presented in Fig. 11(b), and demonstrating that the nonlinear PDM strength and the HF amplitude, can cooperate to induce resonance, is shown in Fig. 12(b). Hence, a bi-harmonically driven PDM system with exponentially varying mass is shown to undergo VR as well as PDM-induced resonance. This is consistent with the results of Roy-Layinde et al. [45] for a PDM system with doubly-singular mass function. However, only single resonances were observed for the exponentially varying mass in contradistinction to the reported double-resonance induced doubly-singular mass function.

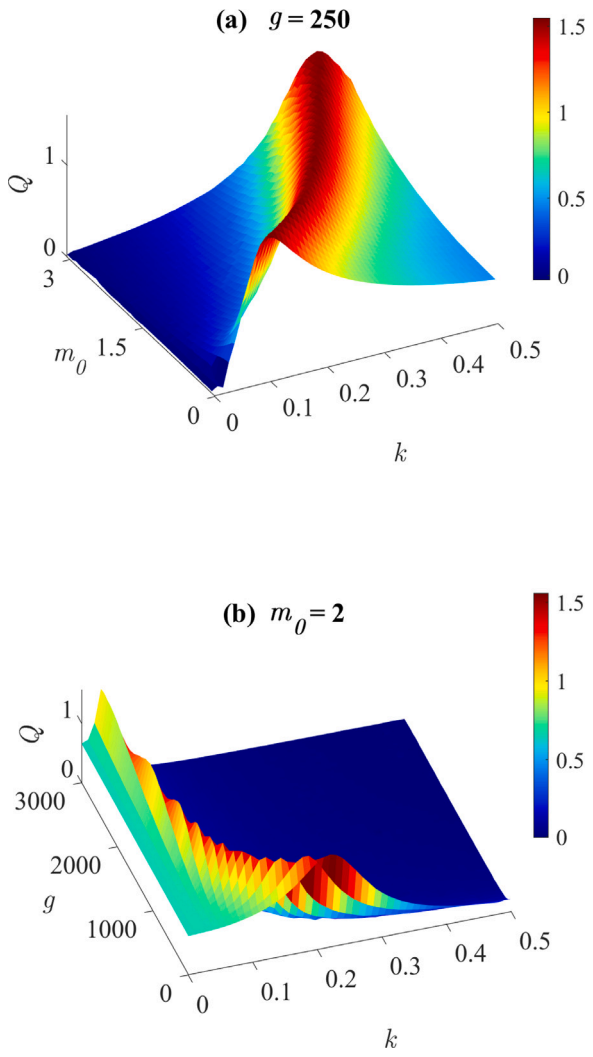

Fig. 12. 3-Dimensional variation of response amplitude Q on mass nonlinear strength k and (a) fixed rest mass m_0 at $g = 250$. Here we chose a wider spectrum of m_0 than that considered in Fig. 11(a) (b) HF amplitude at $m_0 = 2$. We chose a wider spectrum of g than that considered in Fig. 11(b). Other system parameters are: $\beta = 1$, $\alpha = 0.5$, $\omega_0 = 1$, $\omega = 1.3$, $f = 0.1$, $k = 0.01$.

5. Conclusion

Most studies on vibrational resonance focus on systems with constant mass and bi-harmonic drive Motivated by the role of variable-mass in physical systems, we examined vibrational resonance (VR) in a Duffing-type oscillator with exponentially varying position-dependent mass (PDM) and an external driving force. The Duffing-type system was viewed as a driven mechanical system with nonlinear stiffness and periodically-varying mass perturbation. The exponential mass function was modeled as a periodic function of position. The PDM had an inherent accretion process, strong enough to alter the system's rest mass. We considered the cooperation between the PDM parameters comprising a fixed mass m_0 and nonlinear strength k as well as the external high-frequency signal with amplitude g and frequency Ω. Resonance was characterized using the response amplitude Q. Numerical and analytical methods were used to compute the response amplitude. We considered the traditional VR and generated resonance from the HF external signal parameter. It was shown that the observed VR could be controlled by the PDM parameters. Also, we showed that the PDM parameters could be modulated to induce resonance when the system is bi-harmonically driven. In both the observed traditional VR and PDM-induced resonance, single resonances were obtained. The analytical and numerical results are in good agreement with each method being independently sufficient.

The significant cooperation between the PDM and the HF signal, in determining the nature of the observed resonance from the system's response to the particular modulated parameter, was emphasized from theoretical and numerical investigations. The observed PDM-induced resonance effects are similar to those obtained in the traditional VR cases, for a typical constant-mass Duffing oscillator. Clearly, the inherent mass perturbation in the variable mass can play interchangeable roles to the HF periodic signal, leading the system into more controllable and wider resonant states.

CRediT authorship contribution statement

T.O. Roy-Layinde: Conceptualization, Methodology, Investigation, Software, Analysis, Writing – original draft, Writing – reviewing. **K.A. Omoteso:** Methodology, Investigation, Software, Analysis, Writing – original draft, Writing – reviewing. **U.H. Diala:** Methodology, Investigation, Software, Analysis, Resources, Project administration, Supervision, Writing – original draft, Writing – review & editing. **J.A. Runsewe:** Methodology, Investigation, Software, Analysis, Funding. **J.A. Laoye:** Project administration, Resources, Supervision, Software, Validation, Writing – review & editing.

Declaration of competing interest

The authors declare that they have no known competing financial interests or personal relationships that could have appeared to influence the work reported in this paper.

Data availability

No data was used for the research described in the article.

References

[1] Thompson JMT, Stewart HB. Nonlinear dynamics and chaos. John Wiley & Sons; 2002.
[2] Vincent UE, Kolebaje O. Introduction to the dynamics of driven nonlinear systems. Contemp Phys 2020;61(3):169–92.
[3] Fidlin A. Nonlinear oscillations in mechanical engineering. Springer Science & Business Media; 2005.
[4] Bagchi B, Das S, Ghosh S, Poria S. Nonlinear dynamics of a position-dependent mass-driven Duffing-type oscillator. J Phys A 2012;46(3):032001.
[5] Mustafa O. Comment on nonlinear dynamics of a position-dependent mass-driven Duffing-type oscillator. J Phys A 2013;46(36):368001.
[6] von Roos O. Position-dependent effective masses in semiconductor theory. Phys Rev B 1983;27(12):7547.
[7] El-Nabulsi RA. Dynamics of position-dependent mass particle in crystal lattices microstructures. Physica E 2021;127:114525.
[8] Zhao F, Liang X, Ban S. Influence of the spatially dependent effective mass on bound polarons in finite parabolic quantum wells. Eur Phys J B 2003;33(1):3–8.
[9] De Saavedra FA, Boronat J, Polls A, Fabrocini A. Effective mass of one He 4 atom in liquid He 3. Phys Rev B 1994;50(6):4248.
[10] Khordad R. Effect of position-dependent effective mass on linear and nonlinear optical properties in a quantum dot. Indian J Phys 2012;86(6):513–9.
[11] Irschik H, Belyaev AK. Dynamics of mechanical systems with variable mass, vol. 557. Springer; 2014.
[12] Awrejcewicz J. Dynamics of systems of variable mass. In: Classical mechanics. Springer; 2012, p. 341–57.
[13] Nanjangud A, Eke FO. Angular momentum of free variable mass systems is partially conserved. Aerosp Sci Technol 2018;79:1–4.
[14] Cveticanin L. Dynamics of bodies with time-variable mass. Springer; 2016.
[15] Hinvi LA, Koukpémèdji AA, Monwanou VA, Miwadinou CH, Kamdoum Tamba V, Chabi Orou JB. Resonance, chaos and coexistence of attractors in a position dependent mass-driven Duffing-type oscillator. J Korean Phys Soc 2021;1–17.
[16] Karantonis A, Karaoulanis D. Electrical resonance and antiresonance of the electrochemical interface under potentiostatic control: Theoretical considerations. Electrochim Acta 2012;78:244–50.
[17] Gandhimathi V, Rajasekar S, Kurths J. Vibrational and stochastic resonances in two coupled overdamped anharmonic oscillators. Phys Lett A 2006;360(2):279–86.
[18] Rajasekar S, Sanjuan MA. Nonlinear resonances. Springer; 2016.

[19] Buldú JM, Chialvo DR, Mirasso CR, Torrent M, García-Ojalvo J. Ghost resonance in a semiconductor laser with optical feedback. Europhys Lett 2003;64(2):178.
[20] Landa P, McClintock PV. Vibrational resonance. J Phys A: Math Gen 2000;33(45):L433.
[21] Vincent UE, McClintock PV, Khovanov IA, Rajasekar S. Vibrational and stochastic resonances in driven nonlinear systems. 2021.
[22] Jeyakumari S, Chinnathambi V, Rajasekar S, Sanjuán MA. Vibrational resonance in an asymmetric duffing oscillator. Int J Bifurcation Chaos 2011;21(01):275–86.
[23] Chizhevsky V. Vibrational higher-order resonances in an overdamped bistable system with biharmonic excitation. Phys Rev E 2014;90(4):042924.
[24] Roy-Layinde TO, Laoye JA, Popoola OO, Vincent UE, McClintock PVE. Vibrational resonance in an inhomogeneous medium with periodic dissipation. Phys Rev E 2017;96(3):032209.
[25] Vincent UE, Roy-Layinde TO, Adesina PO, Popoola OO, McClintock PVE. Vibrational resonance in an oscillator with an asymmetrical deformable potential. Phys Rev E 2018;98:062203.
[26] Deng B, Wang J, Wei X, Yu H, Li H. Theoretical analysis of vibrational resonance in a neuron model near a bifurcation point. Phys Rev E 2014;89(6):062916.
[27] Yang J, Liu X. Controlling vibrational resonance in a multistable system by time delay. Chaos 2010;20(3):033124.
[28] Yang J, Zhu H. Vibrational resonance in duffing systems with fractional-order damping. Chaos 2012;22(1):013112.
[29] Jothimurugan R, Thamilmaran K, Rajasekar S, Sanjuán MA. Experimental evidence for vibrational resonance and enhanced signal transmission in Chua's circuit. Int J Bifurcation Chaos 2013;23(11):1350189.
[30] Venkatesh P, Venkatesan A. Vibrational resonance and implementation of dynamic logic gate in a piecewise-linear Murali–Lakshmanan–Chua circuit. Commun Nonlinear Sci Numer Simul 2016;39:271–82.
[31] Yu H, Wang J, Liu C, Deng B, Wei X. Vibrational resonance in excitable neuronal systems. Chaos 2011;21(4):043101.
[32] Wu X-X, Yao C, Shuai J. Enhanced multiple vibrational resonances by Na+ and K+ dynamics in a neuron model. Sci Rep 2015;5(1):1–10.
[33] Fu P, Wang C-J, Yang K-L, Li X-B, Yu B. Reentrance-like vibrational resonance in a fractional-order birhythmic biological system. Chaos Solitons Fractals 2022;155:111649.
[34] Rajamani S, Rajasekar S, Sanjuán MAF. Ghost-vibrational resonance. Commun Nonlinear Sci Numer Simul 2014;19(11):4003–12.
[35] Rajasekar S, Sanjuán MAF. Nonlinear resonances. Springer series in synergetics, Switzerland: Springer; 2016.
[36] Liu Y, Dai Z, Lu S, Liu F, Zhao J, Shen J. Enhanced bearing fault detection using step-varying vibrational resonance based on duffing oscillator nonlinear system. Shock Vib 2017.
[37] Zhang D, Yu D. Multi-fault diagnosis of gearbox based on resonance-based signal sparse decomposition and comb filter. Measurement 2017;103:361–9.
[38] Gao J, Yang J, Huang D, Liu H, Liu S. Experimental application of vibrational resonance on bearing fault diagnosis. J Braz Soc Mech Sci Eng 2019;41(1):1–13.
[39] Xiao L, Zhang X, Lu S, Xia T, Xi L. A novel weak-fault detection technique for rolling element bearing based on vibrational resonance. J Sound Vib 2019;438:490–505.
[40] Pan Y, Duan F, Chapeau-Blondeau F, Xu L, Abbott D. Study of vibrational resonance in nonlinear signal processing. Phil Trans R Soc A 2021;379(2192):20200235.
[41] Morfu S, Usama B, Marquié P. On some applications of vibrational resonance on noisy image perception: the role of the perturbation parameters. Phil Trans R Soc A 2021;379(2198):20200240.
[42] Xiao L, Tang J, Zhang X, Xia T. Weak fault detection in rotating machineries by using vibrational resonance and coupled varying-stable nonlinear systems. J Sound Vib 2020;478:115355.
[43] Borromeo M, Marchesoni F. Vibrational ratchets. Phys Rev E 2006;73(1):016142.
[44] Roy-Layinde T, Vincent U, Abolade S, Popoola O, Laoye J, McClintock P. Vibrational resonances in driven oscillators with position-dependent mass. Phil Trans R Soc A 2021;379(2192):20200227.
[45] Roy-Layinde TO, Omoteso KA, Oyero BA, Laoye JA, Vincent UE. Vibrational resonance of ammonia molecule with doubly singular position-dependent mass. Eur Phys J B 2022;95(5):1–11.
[46] Cruz y Cruz S, Rosas-Ortiz O, et al. Dynamical equations, invariants and spectrum generating algebras of mechanical systems with position-dependent mass. SIGMA. Symmetry Integ Geom Methods Appl 2013;9:004.
[47] Plastino AR, Muzzio JC. On the use and abuse of Newton's second law for variable mass problems. Celestial Mech Dynam Astronom 1992;53:227–32.
[48] Roy-Layinde TO, Omoteso KA, Kolebaje OT, Ogunmefun FO, Fasasi RA, Laoye JA, et al. Vibrational resonance in a multistable system with position-dependent mass. Commun Theor Phys 2023;75(11):115602.
[49] Blekhman II. Selected topics in vibrational mechanics, 11, chap. Conjugate resonances and bifurcations of pendulums under biharmonical excitation. In: Chapter: Conjugate Resonances and Bifurcations of Pendulums under Biharmonical Excitation. Singapore: World Scientific Publishing Company; 2004, p. 151–65.
[50] Omoteso KA, Roy-Layinde TO, Laoye JA, Vincent UE, McClintock PV. Delay-induced vibrational resonance in the Rayleigh–Plesset bubble oscillator. J Phys A 2022;55(49):495701.
[51] Blekhman II. Vibrational mechanics: Nonlinear dynamic effects, general approach, applications. World Scientific; 2000.